JCTC Journal of Chemical Theory and Computation

Article

pubs.acs.org/JCTC

Coalescence of Nanoclusters Analyzed by Well-Tempered Metadynamics. Comparison with Straightforward Molecular Dynamics

Lucas M. Farigliano, Sergio A. Paz, Ezequiel P. M. Leiva, and Marcos A. Villarreal*

Departamento de Química Teórica y Computacional, Instituto de Fisicoquímica de Córdoba (INFICQ-CONICET), Universidad Nacional de Córdoba, Córdoba X5000HUA, Argentina

Supporting Information

ABSTRACT: The coalescence process of two nanoparticles to yield a core−shell structure is analyzed by a well-tempered metadynamics procedure. This methodology has been shown to be useful in understanding the present phenomenon in terms of two collective variables: the distance between the center of mass of the coalescing particles and the gyration radius of the resulting core element. The free-energy contour plots clearly show that the coalescence process involves the deformation of the core material, which is manifested in the residence of the system in regions with a larger gyration radius. Results from molecular dynamics for the same system were found helpful to reach the definition of this second collective variable. The advantages and limitations of the latter approach are discussed.

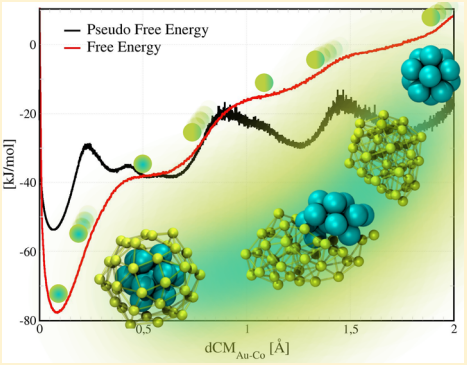

1. INTRODUCTION

Within the universe of nanoparticles, systems composed of two metallic elements (bimetallic nanoparticles, BM-NPs) have been widely studied because they show a great variety of physicochemical properties.[1−4] Among the different ways to prepare BM-NPs the coalescence processes provide an interesting alternative to high speed synthesis. Coalescence constitutes a particular case of collisions where the impact speed between the NPs tends to zero. These processes play a dominant role in the formation of new clusters for a wide range of experimental conditions in contrast with the processes of high-speed collisions which require more sophisticated experimental designs.[1,2,4,5]

Concerning the computational study of the coalescence processes, straightforward molecular dynamics simulations (MD) have been previously reported.[6−11] Paz et al.[11] performed MD coalescence studies at high temperatures using nanoparticles (NPs) made of a few atoms; both conditions are necessary to make the simulations feasible with ordinary computational tools. From those results, the authors presented a new methodology of analysis based on the construction of pseudo-free-energy profiles (pFEP), which has been shown to be useful in the characterization of the processes studied. In contrast with the standard methods to recover the Landau free-energy,[12,13] the methodology of Paz et al. uses statistics from hundreds of nonequilibrium MD simulations to accumulate histograms which are used to analyze the occurrence of bottlenecks during an irreversible nonequilibrium process. We emphasize that the present coalescence process is intrinsically irreversible: the resulting core−shell structure remains stable within the experimental time scale.

Despite the predictive power of MD simulations, the observation of one or a set of paths on the phase space may not be sufficient for the statistical convergence of the requested observable which is frequently compared with experimental results obtained in the time scale of seconds or more. Depending on the system size, first-principles MD usually reach time scales of a few picoseconds and classical MD hundreds of nanoseconds or a few microseconds. There are many ways to study the coalescence processes beyond brute-force MD simulations. For example, by giving up the all-atom description it is possible to reach larger time scales using coarse-grain models.[14] On the other hand, if the atomistic description is not to be omitted, methodologies able to accelerate rare events can be applied to improve the computational efficiency. For example, there are many methods aimed to enhance the sampling of the probability distribution along a few selected degrees of freedom or collective variables (CVs). Usually, these methods also allow the reconstruction of the corresponding free-energy landscape giving a decrease in the dimensionality of the problem, as suggested by Kevrekidis.[15,16] Among these methods we can mention umbrella sampling,[17,18] conformational flooding,[19] weighted histogram techniques,[20−22] Jarzynski's identity-based methods,[23,24] adaptive force bias,[25,26] steered MD,[27] adiabatic

Received: February 13, 2017
Published: June 28, 2017

DOI: 10.1021/acs.jctc.7b00151
J. Chem. Theory Comput. XXXX, XXX, XXX−XXX

molecular dynamics,[28] and well-tempered metadynamics (WTMD).[29]

The WTMD method enhances the configurational sampling by adding a repulsive history-dependent potential along a set of few CVs.[29] This potential discourages the system from assuming repeatedly the same value of the CVs, thus effectively increasing the scope of exploration of the configuration space. A proper choice of the history-dependent potential provides an increased sampling rate of rare events and an estimate of the free-energy profile (FEP) along the chosen CVs. An important difficulty in the implementation of WTMD is the requirement that the CVs should provide a good representation of the reaction coordinate. That is, the chosen CVs have to be able to describe the process of interest. If one of the relevant modes is not reproduced by the CVs, CV-biased free-energy methods as WTMD may suffer hysteresis, and the analysis can fall into serious convergence issues.[30,31] The addition of the missing mode as a new CV constitutes a solution to this problem, but, if the set of CVs increases, the computational demand will concomitantly increase as a function of the number of variables.

In the present work, we use WTMD to perform a thorough sampling of the configurations involved in the coalescence process of cobalt (Co) and gold (Au) nanoparticles. This system is prototypical for core−shell formation studies. Previous reports by some of us[11] and others[32−35] are reported in the bibliography.

The CVs of choice are inferred from the pseudo-free-energy profiles previously constructed for this process. A critical comparison is made between the information resulting from these pseudo-free-energy profiles (nonequilibrium) calculated as in our previous work[11] with the free-energy profiles emerging from the present equilibrium methodology, with an emphasis on the different types of information that can be obtained with both methodologies.

2. METHODOLOGY

As stated in the Introduction, different methodologies were developed throughout the years to overcome the limitations of MD simulations. The current choice is WTMD, where the evolution of a system is biased by a history-dependent potential, constituted by a sum of Gaussian functions. The gaussians are deposited along the trajectory of the system in the free-energy space of the CVs chosen for the process under consideration. After the simulation converge, this potential is used for the reconstruction of the free-energy profile as a function of the CVs.

For a system evolving without a bias, the FEP is a function of its degrees of freedom $s(q)$, where q represents the coordinates of the system, according to

$$F(s) = -T \lim_{t\to\infty} \ln(N(s, t)) \tag{1}$$

where $N(s, t) = \int_0^t \delta_{s,\tilde{s}(t')} dt'$ is a histogram of the variable s, and T is the temperature. To improve the sampling, a history-dependent bias potential $V(s, t)$ is incorporated to the potential energy according to

$$V(s, t) = \Delta T \ln \frac{\omega N(s, t)}{\Delta T} \tag{2}$$

where ω has units of an energy rate, ΔT has units of a temperature, and $N(s, t)$ stems from the Gaussian deposition during the simulation.

At the time of analyzing the performance of the methodology, a quantity of major importance is the rate at which the potential bias is modified, that is, the rate at which new Gaussian functions are incorporated into the bias potential. The slower the rate at which these gaussians are incorporated, the closer the system dynamics will be to the thermodinamic equilibrium.

The main difference of WTMD with its parent technique, metadynamics, is the fact that the height of the Gaussian functions is varied along the simulation, according to the rate $w = \omega e^{-\frac{V(s,t)}{\Delta T}} \tau_G$, where τ_G is the time interval at which the gaussians are deposited. At long times, $V(s, t)$ varies very slowly, leading to a distribution probability approaching equilibrium according to

$$P(s, t)ds \propto e^{-\frac{F(s)+V(s,t)}{T}} ds \tag{3}$$

According to the previous equation and the potential bias described previously, the estimation $\tilde{F}(s, t)$ of the free-energy surface is

$$\tilde{F}(s, t) = -\frac{T + \Delta T}{\Delta T} V(s, t) \tag{4}$$

One of the main assumptions made for the free-energy analysis is that the microstates relevant for the system are well described by the set of CVs chosen. For the present system, our choice for the CVs is the distance between the centers of mass of the NPs, $d\mathrm{CM}_{\mathrm{Au-Co}}$, and the gyration radius of the Co cluster, $\mathrm{Rg}_{\mathrm{Co}}$.

The center of mass of each of the nanoparticles is given by $\overrightarrow{\mathrm{CM}_i} = \frac{1}{M_i} \sum_{j=1}^{n} m_j \vec{x}_j$, where m_j is the mass of the atom j, x_j is its position, and M_i is the total mass of the NP under consideration. In this way the distance between the centers of mass is given by

$$d\mathrm{CM}_{\mathrm{Au-Co}} = \overrightarrow{\mathrm{CM}_{\mathrm{Au}}} - \overrightarrow{\mathrm{CM}_{\mathrm{Co}}} \tag{5}$$

$d\mathrm{CM}_{\mathrm{Au-Co}}$ allows for the following of the different stages occurring during coalescence. This CV acquires a high value at the initial state, corresponding to separated NPs, and it reaches a minimum value close to zero at the final state. Figure 1 shows representations of both extremes of the coalescence process. The final state of the present irreversible process corresponds to an icosahedral bimetallic NP, with a core−shell structure where the Co atoms constitute the core and the Au atoms

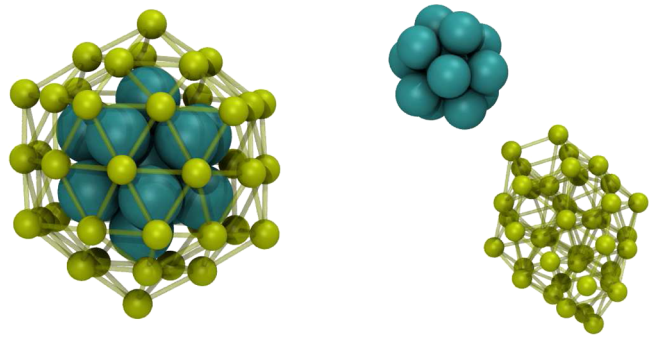

Figure 1. Typical snapshots of the initial (right) and final (left) states of the coalescence phenomenon considered here. Co atoms are represented in blue, and Au atoms are represented in yellow. A core−shell structure can be observed in the figure on the left.

DOI: 10.1021/acs.jctc.7b00151
J. Chem. Theory Comput. XXXX, XXX, XXX−XXX

constitute the shell. Note that WTMD does not distinguish between initial and final configurations of the simulation, as all the allowed values of the CV are visited several times as the simulation proceeds (see for example Supporting Informationn Figure S1). Our reference to initial and final states is in relation to the order they appear in the MD simulations.

The gyration radius Rg_{Co} provides a measure for the sphericity of the Co cluster, and its square is given by

$$Rg^2 = \frac{1}{n}\sum_{i=1}^{n}(\vec{x_i} - \overrightarrow{CM_{Co}})^2 \quad (6)$$

where $\overrightarrow{CM_{Co}}$ is the center of mass defined above. Rg_{Co} allows for the distinguishing of configurations with the same $d\mathrm{CM}_{Au-Co}$ and different sphericities of the core. This secondary CV allows for the description of the coalescence process in finer detail.

According to the previous discussion, the results presented here correspond to a two-dimensional WTMD (WTMD-2D), in which the optimized parameters were the energy rate ω, the Gaussian parameters of the two collective variables, say $\sigma_{d\mathrm{CM}_{Au-Co}}$ and $\sigma_{Rg_{Co}}$, the damping parameter ΔT, and the time interval τ_G. The values used here were as follows: ω = 0.5 kJ/mol, $\sigma_{d\mathrm{CM}_{Au-Co}}$ = 0.002 Å, $\sigma_{Rg_{Co}}$ = 0.001 Å, ΔT = 3000 K, τ_G = 500 fs. The spatial resolution and the computational time of metadynamics are sensible to these parameters. We have explored different parameter values around those usually suggested by the method[36−38] and finally choose those that give us a converged free-energy profile within a reasonable computational time.

To provide a more detailed description of the FEP in the region of interest, the system was confined by the following repulsive bias potentials

$$\mathrm{Pot}_{rep} = \begin{cases} \frac{1}{2}k_{rep}(\mathrm{CVs}_i - \mathrm{CVs}_{\min_i})^2 & \text{if } \mathrm{CVs}_i < \mathrm{CVs}_{\min_i} \\ 0 & \text{if } \mathrm{CVs}_{\min_i} \le \mathrm{CVs}_i \le \mathrm{CVs}_{\max_i} \\ \frac{1}{2}k_{rep}(\mathrm{CVs}_i - \mathrm{CVs}_{\max_i})^2 & \text{if } \mathrm{CVs}_i > \mathrm{CVs}_{\max_i} \end{cases} \quad (7)$$

where k_{rep} is a force constant, and $\mathrm{CVs}_{\min_i}$ and $\mathrm{CVs}_{\max_i}$ represent the minimum and maximum values where the present potential is zero for the CVs_i.

Besides the WTMD analysis, the clustering of nonequilibrium trajectories was used to calculate pseudo-free-energy profiles $F'(s)$ and compare them with previous work.[11] Two hundred MD runs with different starting condition simulations were launched for this purpose. The basic idea of this methodology focuses on the study of the probability $P'(s)$ of visiting microstates during an irreversible process. This is constructed from histograms obtained using MD trajectories generated in the canonical ensemble. Thus, we have

$$F'(s) = -kT \ln (P'(s)) \quad (8)$$

As mentioned in the Introduction the coalescence process is a particular case of collisions where the impact speeds tend to zero. This process might take place on different environments, from liquid solutions to solid surfaces.[3,4,39] For this reason we choose to model the system in the canonical ensemble which reflects the energy exchange with the surroundings. It should be noted that if the interest is on the simulation of high speed collisions as in ref 40, the microcanonical ensemble would be a better choice since it reflects more appropriately the experimental settings that involve high vacuum.

This methodology has been found useful to identify the microstates that are relevant during the formation of the core−shell (Figure 1). An interesting question that arises is whether the information that can be obtained used WTMD can be correlated with that stemming from the pFEP analysis.

The interaction potential used to describe the interaction between the particles of the system is the second-neighbors tight binding potential, with the same parameters as those of ref 32. The equations of motion were integrated using Ermak's algorithm at 550 K with a viscosity of 5 ps/Å. In the case of the pFEP analysis, the collective variable used was $d\mathrm{CM}_{Au-Co}$.

In the search for a direct relationship between FEP and pFEP, 1D Langevin dynamics simulations were performed using as potential energy the 2D free-energy profile obtained from the WTMD-2D. 500 Langevin MD simulations were launched starting at $d\mathrm{CM}_{Au-Co}$ = 11 Å, using 150000 integration steps of 0.1 fs at 550 K, with a friction coefficient of 500 ps^{-1}.

3. RESULTS AND DISCUSSION

Similarly to the illustration in Figure 1, the systems were initially separated by a distance close to 11.5 Å between the centers of mass, ending with a separation close to 0 Å at the final state.

A key aspect in the simulations to check the convergence of the free-energy profiles is the behavior of the CVs involved in the simulation. Early runs using WTMD with $d\mathrm{CM}_{Au-Co}$ as unique CV led to poorly converged results due to hysteretic behavior (strongly indicative that an important CV was missing). There is not a priori method for finding the correct set of CVs, and in many cases it is necessary to proceed by trial and error. In this context, a second CVs, Rg_{Co}, in eq 2 was introduced. The monitoring of the two CVs shows a good diffusive behavior over a long time in both directions of the energy plane, $d\mathrm{CM}_{Au-Co}$ and Rg_{Co} (Figure S1, Supporting Information (SI)). The reason for using Rg_{Co} as a second CV is based on the long-lived metastable state detected in ref 11. This state has a configuration similar to the final core−shell configuration, but it has a Co atom from the core exchanged with an Au atom from the shell. Introducing the CVs in the WTMD-2D scheme allows for the sampling of the expanded structures of the system close to the final configuration, favoring atom exchange and avoiding the trapping in the metastable state. Figure 2 shows a snapshot of one of these trapped states, where a Co atom of the core has been exchanged with a Au atom from the shell. The resulting structure defines a slightly distorted icosahedron.

Figure 3a shows the 2D free-energy profile of the coalescence process between 0.0 and 13.9 Å in $d\mathrm{CM}_{Au-Co}$ and 2.2 and 2.8 Å in Rg_{Co}, as obtained from WTMD. From this figure it can be seen that the minimum free-energy path for the coalescence process presents a slight increase in the value of the Rg_{Co} CV compared to the value registered for the separated nanoparticles (initial state). On the other hand, when approaching the final state of the process (core−shell) the system seems to decrease the value of the auxiliary variable to conform the heart of the nanoparticle with the atoms of Co.

Figure 3b shows a zoom of the 2D free-energy profile in the region confined by the repulsive walls between 0.0 and 2.0 Å in $d\mathrm{CM}_{Au-Co}$ and 2.2 and 2.8 Å in Rg_{Co}. While Figure 3a shows a

DOI: 10.1021/acs.jctc.7b00151
J. Chem. Theory Comput. XXXX, XXX, XXX−XXX

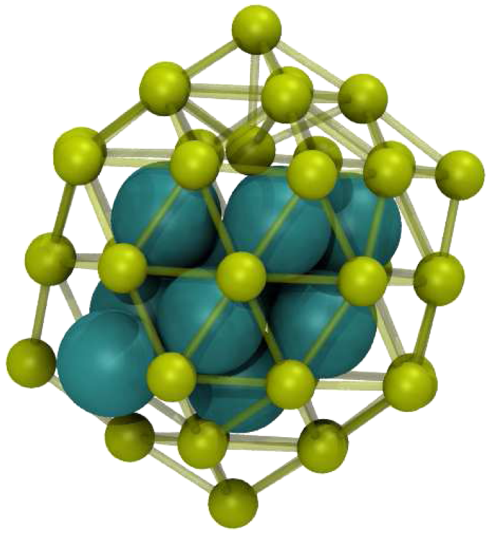

Figure 2. Sample configuration of a "trapped state" for the Co−Au system. The core is made of 12 Co atoms and 1 Au atom.

monotonic growth of the energy with $d\mathrm{CM}_{\mathrm{Au-Co}}$, Figure 3b allows for the determination of a sharp minimum at $d\mathrm{CM}_{\mathrm{Au-Co}}$ = 0.1 Å and $\mathrm{Rg}_{\mathrm{Co}}$ = 2.38 Å. This minimum corresponds to the final core−shell structure of the system, the most commonly visited conformation. On the other hand, a slightly pronounced free-energy minimum appears at $d\mathrm{CM}_{\mathrm{Au-Co}}$ = 0.6 Å and $\mathrm{Rg}_{\mathrm{Co}}$ = 2.52 Å, which corresponds to trapped states already reported in the literature.[11] Shallow regions can also be noted at values close to $d\mathrm{CM}_{\mathrm{Au-Co}}$ = 1.0 Å.

The present choice of the second collective variable was allowed to prevent the hysteresis found in the $d\mathrm{CM}_{\mathrm{Au-Co}}$ analysis, yielding properly converged results. In order to compare these results with the pseudo-free-energy previously obtained, we need to project the two-dimensional FEP reconstructed via WTMD onto the one-dimensional space of the $d\mathrm{CM}_{\mathrm{Au-Co}}$ CVs. Thus, we define the quantity $F_{\mathrm{proy}}(d\mathrm{CM}_{\mathrm{Au-Co}})$ according to the following equation

$$F_{\mathrm{proy}}(d\mathrm{CM}_{\mathrm{Au-Co}}) = \sum_{i=\mathrm{Rg}_{\mathrm{Co_{min}}}}^{i=\mathrm{Rg}_{\mathrm{Co_{max}}}} P(d\mathrm{CM}_{\mathrm{Au-Co}}, i) \tag{9}$$

where $P(d\mathrm{CM}_{\mathrm{Au-Co}}, i)$ is the probability of observing a pair of values ($d\mathrm{CM}_{\mathrm{Au-Co}}$, $\mathrm{Rg}_{\mathrm{Co}}$) within the free-energy map. In eq 9, the limits of the sum correspond to the values of $\mathrm{Rg}_{\mathrm{Co}}$ where the repulsive barriers have been set.

The result of the projection of the 2D free-energy profiles of the process onto $d\mathrm{CM}_{\mathrm{Au-Co}}$ is shown in Figure 4. In this figure, it can be observed that the one-dimensional profile presents a single minimum at small $d\mathrm{CM}_{\mathrm{Au-Co}}$ distances (∼0.1 Å) and different plateaus at about 0.6, 1.2, and 1.7 Å.

Under these conditions, a straightforward comparison between the FEP and pFEP methodologies can be made. It is remarkable that the pFEP present minima around 0.1, 0.6, 1.25, and 1.75 Å (see Figure 5). That is, while the deep minimum coincides for both methodologies, the arrests observed in Figure 4 show a close cut correlation with the secondary minima of the pFEP. In other words, the most visited configurations are the same in both cases, though highlighted in a different way. However, a limitation in the prediction of the pFEP representation must be discussed as follows. Since straightforward MD is not able to explore configurations far

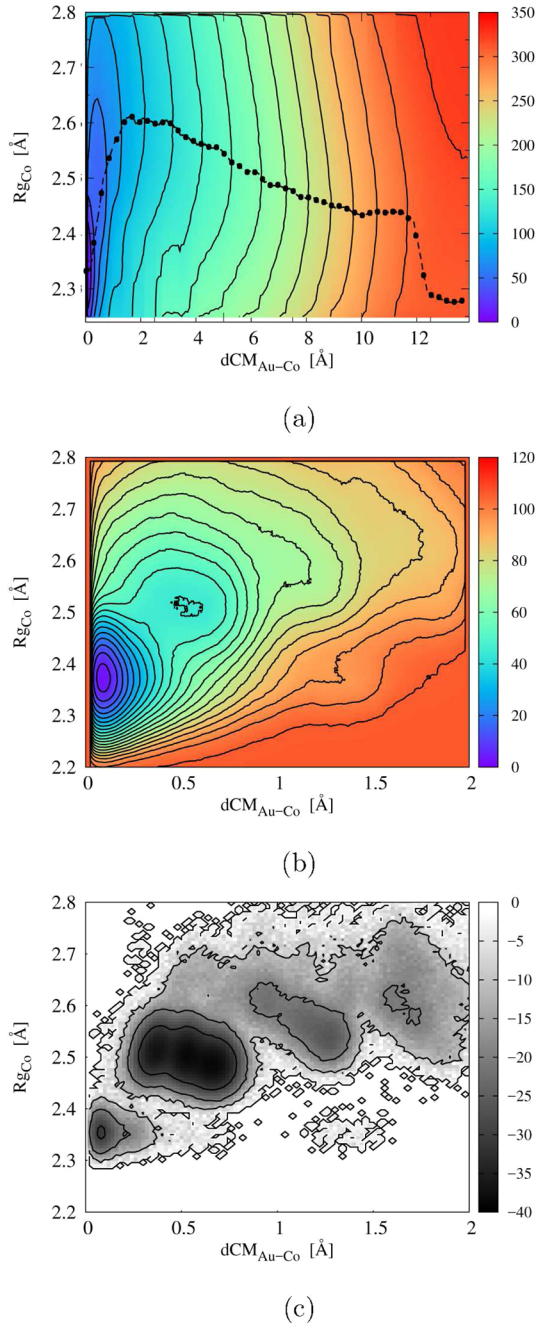

Figure 3. (a) Free-energy contour plot of the coalescence process in the $\mathrm{Rg}_{\mathrm{Co}}$ vs $d\mathrm{CM}_{\mathrm{Au-Co}}$ plane. The minimum free-energy path is shown. (b) Like (a) but using repulsive walls $\mathrm{Rg}_{\mathrm{Co}}$ = 2.2 and 2.8 Å and $d\mathrm{CM}_{\mathrm{Au-Co}}$ = 0.0 and 2.0 Å. (c) Pseudo-free-energy contour plot constructed from MD trajectories starting at $d\mathrm{CM}_{\mathrm{Au-Co}} \approx 11.5$ Å and $\mathrm{Rg}_{\mathrm{Co}} \approx 2.3$ Å. This data corresponds to those shown in the black curve of Figure 5.

from the global minimum, once the system has reached this location the results may be strongly vitiated if the simulation is pursued for a long time in this region. To show this fact more clearly, we have analyzed different MD trajectories where the criteria to finish the simulation were varied. On the one hand, the MD trajectories were stopped when $d\mathrm{CM}_{\mathrm{Au-Co}}$ was smaller than 0.1 Å. This is shown in the black curve of Figure 5 and yields results similar to those of the literature, where the simulation was stopped at $d\mathrm{CM}_{\mathrm{Au-Co}} < 3.10^{-2}$ Å, green curve. On the other hand, the simulations were further pursued for a

DOI: 10.1021/acs.jctc.7b00151
J. Chem. Theory Comput. XXXX, XXX, XXX−XXX

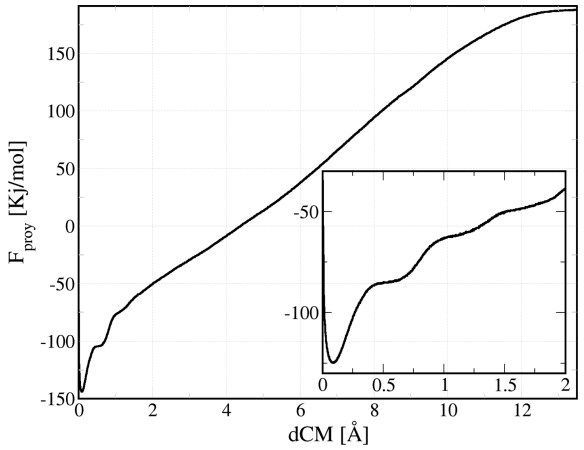

Figure 4. Free-energy as a function of dCM_{Au-Co}, obtained according to eq 9. The inset shows a magnification in the region between 0 and 2 Å.

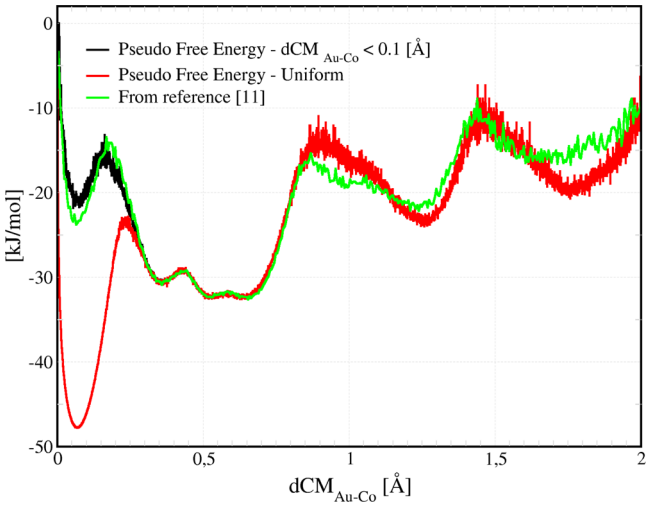

Figure 5. Pseudo-free-energy profiles as a function of dCM_{Au-Co}, using different criteria to end the simulations, as discussed in the text. The black and green curves correspond to simulations stopped when $dCM_{Au-Co} < 0.1$ Å and $dCM_{Au-Co} < 3.10^{-2}$ Å, respectively. The red curve corresponds to a simulation performed for a total simulation time of 1250.0 ns (uniform), setting no restriction on dCM_{Au-Co}.

total simulation time of 1250 ns, with the results shown in the red curve of Figure 5. In the latter case, it is evident that the permanence of the system in regions where dCM_{Au-Co} is close to zero results in a deepening of the pFEP in this region, so encumbering any conclusions on the relative stability of the different structures.

The previous results show that some criteria for finishing the MD simulation must be used within the pFEP to prevent overemphasizing the final core−shell configuration. Thus, a general conclusion is that the pFEP yields information on the occurrence of the different structures which are relevant on the way to the formation of the core−shell structure, but their relative stability requires a deeper thermodynamic analysis as the present one.

As mentioned above, the convergence of FEP profiles within the WTMD depends strongly on the choice of the set of collective variables under which we can find converged results. For this reason, it is very important to choose from these CVs. In this sense, there are many methodologies that allow the acceleration in the spaces of the CVs. One of them is temperature-accelerated molecular dynamics (TAMD),[41] where the sampling is made over a large number of CVs.[42−45] However, the direct appreciation of a free-energy profile within a sampling performed in a 69-dimensional space is beyond human capabilities.[42] Therefore, there is a compromise between using a large set of CVs that properly describes the system and the difficulty of finding a minimum set of CVs which sheds light onto the process taking place, where all the slow modes of the system must be taken into account. If one of these modes is not included in the definition of the set, then hidden barriers in the space of the CVs can appear, greatly affecting the sampling efficiency.[46−48] In this context, the methodologies used to obtain FEP and pFEP are complementary. The pFEP allowed the detection of trapped states and was able to characterize them regardless of whether the CV used is a good collective variable for the WTMD. In this sense, the pFEPs were found useful to solve the problem of hysteresis in the WTMD, since they allowed the definition of a collective variable that helped to leave trapped states.

It is also worth mentioning that according to the WTMD-2D no barriers exist for the formation of the core−shell but rather regions where the process is slowed down. Figure 3c shows the pFEP calculated from the MD trajectories, which may be compared with the free-energy profiles of Figure 3b. The minima observed in the one-dimensional plot of Figure 5 become evident, although it can be seen that they are distributed along the Rg_{Co} axis. These minima are denoted by the more obscure regions in the figure, representing the more often visited coordinates. According to these results, the mostly visited coordinates correspond to the region defined by the segments [2.4, 2.6] Å in Rg_{Co} and [0.4, 0.7] Å in dCM_{Co-Au}. This straightforward comparison between the pFEP (Figure 3c) and the FEP (Figure 3b) allows us to draw two important conclusions. First, both landscapes present a minimum corresponding to the core−shell at the same point (Rg_{Co},dCM_{Co-Au}). Second, in those regions where the pFEP presents other minima, WTMD-2D presents plateaus, revealing the most relevant structures occurring on the way to the formation of the core−shell structure. The formation of the core−shell structures does not follow a straight trajectory along the dCM_{Co-Au} but describes a bow involving an increase in the Rg_{Co} coordinate.

In order to further explore the connection between the pFEP and the FEP, the motion of a 1D particle was simulated using the projection of the FEP onto the dCM_{Co-Au} as the potential energy. Using Langevin dynamics the pFEP was constructed for this 1D particle, and it is shown by the black line of Figure 6. Noteworthily, the obtained pFEP presents a structure of maxima and minima that reflects the same behavior of the original pFEP constructed for the coalescence system (red curve in Figure 6). The emergence of this maxima and minima from the 1D Langevin dynamics, which is run on a potential energy profile where maxima and minima are absent, indicates that these extrema in the pFEP are a consequence of the arrest (*plateaus*) in the FEP.

Finally, it is pertinent to mention that there is a great deal of literature on NP coalescence studied by ordinary molecular dynamics[49−53] and specifically on binary NPs.[40,54−56] In many of them, emphasis is given to metastable configurations, defect occurrence, influence of relative orientation, temperature, materials, size, etc. While kinetic issues cannot be strictly addressed with the present methodology, the occurrence of

DOI: 10.1021/acs.jctc.7b00151
J. Chem. Theory Comput. XXXX, XXX, XXX−XXX

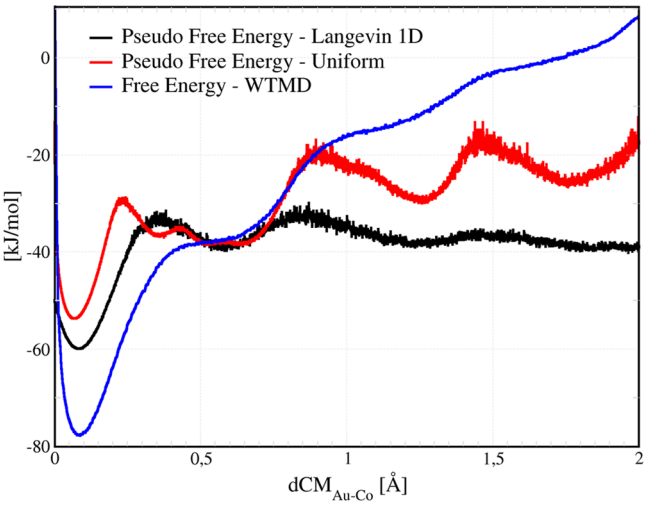

Figure 6. Comparison between different quantities averaged along the coordinate representing the distances between the centers of mass of the coalescing nanoparticles. Blue: Projection of the WTMD free-energy profile. Red: Pseudo-free-energy profiles obtained from ordinary molecular dynamics. Black: Pseudo-free-energy profiles obtained from Langevin dynamics. The effective potential for the latter was obtained from the projection of the free-energy profiles onto the $d\mathrm{CM}_{\mathrm{Co-Au}}$ coordinate.

metastable states could be recognized by inspection of free-energy landscapes, like those shown in Figure 3a and b. On the other hand, 1-D free-energy profiles may be further useful to recognize if the occurrence of situations where the system stays for a relative long time is due to a metastable state (i.e. a local minimum in the configuration space) or if we are dealing with situations where the coalescence process is just slowed down (inflection points).

4. CONCLUSION

We have analyzed the coalescence process of two nanoparticles by a well-tempered metadynamics procedure. This methodology has been shown to be very useful in understanding the present phenomenon, in terms of two collective variables. While one of them, the distance between the center of mass of the coalescing particles, was relatively straightforward to infer, the other one, the gyration radius, was less obvious. The free-energy contour plots clearly show that the coalescence process involves the deformation of the core material, which is manifest in the residence of the system in regions with a larger gyration radius.

Results from molecular dynamics for the same system were helpful to arrive to the definition of the second collective variable. However, where the free-energy landscape exhibits subtle plateaus, pseudo-free-energy profiles obtained from molecular dynamics suggested significant trapped (metastable) states. The apparent contradiction between both (MD and WTMD) results was elucidated by the Langevin dynamics of a 1D particle over the free-energy surface, inviting increased attention to some free-energy features that might be often overlooked.

■ ASSOCIATED CONTENT

Supporting Information

The Supporting Information is available free of charge on the ACS Publications website at DOI: 10.1021/acs.jctc.7b00151.

Figure S1, behavior of the collective variables as a function of the simulation time (PDF)

■ AUTHOR INFORMATION

Corresponding Author

*E-mail: mvillarreal@unc.edu.ar.

ORCID

Lucas M. Farigliano: 0000-0002-8728-1276

Notes

The authors declare no competing financial interest.

■ ACKNOWLEDGMENTS

This work was supported by PIP CONICET-11220110100992, Program BID-FONCyT PICT-2012-2324, SECyT UNC. This work was performed at INFICQ-CONICET and Facultad de Ciencias Químicas, Universidad Nacional de Córdoba, Argentina.

■ REFERENCES

(1) Mariscal, M. M.; Mayoral, A.; Olmos-Asar, J. A.; Magen, C.; Mejía-Rosales, S.; Pérez-Tijerina, E.; José-Yacamán, M. Nanoalloying in real time. A high resolution STEM and computer simulation study. *Nanoscale* **2011**, *3*, 5013−5019.

(2) Zheng, H.; Smith, R. K.; Jun, Y.; Kisielowski, C.; Dahmen, U.; Alivisatos, A. P. Observation of Single Colloidal Platinum Nanocrystal Growth Trajectories. *Science* **2009**, *324*, 1309−1312.

(3) Liu, H.; José-Yacaman, M.; Perez, R.; Ascencio, J. Studies of nanocluster coalescence at high temperature. *Appl. Phys. A: Mater. Sci. Process.* **2003**, *77*, 63−67.

(4) José-Yacamán, M.; Gutierrez-Wing, C.; Miki, M.; Yang, D.; Piyakis, K. N.; Sacher, E. Surface Diffusion and Coalescence of Mobile Metal Nanoparticles. *J. Phys. Chem. B* **2005**, *109*, 9703−9711.

(5) Colliex, C. Watching Solution Growth of Nanoparticles in Graphene Cells. *Science* **2012**, *336*, 44−45.

(6) Wang, J.; Chen, S.; Cui, K.; Li, D.; Chen, D. Approach and Coalescence of Gold Nanoparticles Driven by Surface Thermodynamic Fluctuations and Atomic Interaction Forces. *ACS Nano* **2016**, *10*, 2893−2902.

(7) Goudeli, E.; Pratsinis, S. E. Crystallinity dynamics of gold nanoparticles during sintering or coalescence. *AIChE J.* **2016**, *62*, 589−598.

(8) Grammatikopoulos, P.; Toulkeridou, E.; Nordlund, K.; Sowwan, M. Simple analytical model of nanocluster coalescence for porous thin film design. *Modell. Simul. Mater. Sci. Eng.* **2015**, *23*, 015008.

(9) Zhang, Y.; Feng, G.; Gao, X.; Zhou, S. Coalescence of ZnSe Nanoparticles: Molecular Dynamics Study. *J. Comput. Theor. Nanosci.* **2014**, *11*, 1766−1772.

(10) Guevara-Chapa, E.; Mejía-Rosales, S. Molecular dynamics of coalescence and collisions of silver nanoparticles. *J. Nanopart. Res.* **2014**, *16*, 1−10.

(11) Paz, S. A.; Leiva, E. P. Unveiling the mechanism of core-shell formation by counting the relative occurrence of microstates. *Chem. Phys. Lett.* **2014**, *595*−*596*, 87−90.

(12) Wales, D. *Energy Landscapes: Applications to Clusters, Biomolecules and Glasses*; Cambridge University Press: Cambridge, 2001.

(13) *Free Energy Calculations: Theory and Applications in Chemistry and Biology*; Chipot, C., Pohorille, A., Eds.; Springer: 2007; DOI: 10.1007/978-3-540-38448-9.

(14) Brennan, J. K.; Lísal, M. Coarse-grain models for metals: Constant-pressure dissipative dynamics simulations. *Proceedings - 14th International Detonation Symposium, IDS 2010* **2010**, 1451−1459.

(15) Theodoropoulos, C.; Qian, Y. H.; Kevrekidis, I. G. "Coarse" stability and bifurcation analysis using time-steppers: A reaction-diffusion example. *Proc. Natl. Acad. Sci. U. S. A.* **2000**, *97*, 9840−9843.

(16) Kevrekidis, I. G.; Gear, C. W.; Hummer, G. Equation-free: The computer-aided analysis of complex multiscale systems. *AIChE J.* **2004**, *50*, 1346−1355.
(17) Torrie, G.; Valleau, J. Nonphysical sampling distributions in Monte Carlo free-energy estimation: Umbrella sampling. *J. Comput. Phys.* **1977**, *23*, 187−199.
(18) Kumar, S.; Rosenberg, J. M.; Bouzida, D.; Swendsen, R. H.; Kollman, P. A. THE weighted histogram analysis method for free-energy calculations on biomolecules. I. The method. *J. Comput. Chem.* **1992**, *13*, 1011−1021.
(19) Grubmüller, H. Predicting slow structural transitions in macromolecular systems: Conformational flooding. *Phys. Rev. E: Stat. Phys., Plasmas, Fluids, Relat. Interdiscip. Top.* **1995**, *52*, 2893−2906.
(20) Ferrenberg, A. M.; Swendsen, R. H. New Monte Carlo technique for studying phase transitions. *Phys. Rev. Lett.* **1988**, *61*, 2635−2638.
(21) Kumar, S.; Rosenberg, J. M.; Bouzida, D.; Swendsen, R. H.; Kollman, P. A. Multidimensional free-energy calculations using the weighted histogram analysis method. *J. Comput. Chem.* **1995**, *16*, 1339−1350.
(22) Roux, B. The calculation of the potential of mean force using computer simulations. *Comput. Phys. Commun.* **1995**, *91*, 275−282.
(23) Jarzynski, C. Nonequilibrium Equality for Free Energy Differences. *Phys. Rev. Lett.* **1997**, *78*, 2690−2693.
(24) Crooks, G. E. Nonequilibrium Measurements of Free Energy Differences for Microscopically Reversible Markovian Systems. *J. Stat. Phys.* **1998**, *90*, 1481−1487.
(25) Darve, E.; Pohorille, A. Calculating free energies using average force. *J. Chem. Phys.* **2001**, *115*, 9169−9183.
(26) Rodriguez-Gomez, D.; Darve, E.; Pohorille, A. Assessing the efficiency of free energy calculation methods. *J. Chem. Phys.* **2004**, *120*, 3563−3578.
(27) Gullingsrud, J. R.; Braun, R.; Schulten, K. Reconstructing Potentials of Mean Force through Time Series Analysis of Steered Molecular Dynamics Simulations. *J. Comput. Phys.* **1999**, *151*, 190−211.
(28) Rosso, L.; Minárý, P.; Zhu, Z.; Tuckerman, M. E. On the use of the adiabatic molecular dynamics technique in the calculation of free energy profiles. *J. Chem. Phys.* **2002**, *116*, 4389−4402.
(29) Barducci, A.; Bussi, G.; Parrinello, M. Well-Tempered Metadynamics: A Smoothly Converging and Tunable Free-Energy Method. *Phys. Rev. Lett.* **2008**, *100*, 020603.
(30) Barducci, A.; Parrinello, M.; Bonomi, M. Metadynamics. *Wiley Interdiscip. Rev. Comput. Mol. Sci.* **2011**, *1*, 826−843.
(31) Paz, S. A.; Abrams, C. F. Free Energy and Hidden Barriers of the β-Sheet Structure of Prion Protein. *J. Chem. Theory Comput.* **2015**, *11*, 5024−5034.
(32) Rapallo, A.; Olmos-Asar, J. A.; Oviedo, O. A.; Ludueña, M.; Ferrando, R.; Mariscal, M. M. Thermal Properties of Co/Au Nanoalloys and Comparison of Different Computer Simulation Techniques. *J. Phys. Chem. C* **2012**, *116*, 17210−17218.
(33) Mayoral, A.; Mejia-Rosales, S.; Mariscal, M. M.; Perez-Tijerina, E.; Jose-Yacaman, M. The Co-Au interface in bimetallic nanoparticles: a high resolution STEM study. *Nanoscale* **2010**, *2*, 2647−2651.
(34) Wen, T.; Krishnan, K. M. Cobalt-based magnetic nanocomposites: fabrication, fundamentals and applications. *J. Phys. D: Appl. Phys.* **2011**, *44*, 393001.
(35) Llamosa Pérez, D.; Espinosa, A.; Martínez, L.; Román, E.; Ballesteros, C.; Mayoral, A.; García-Hernández, M.; Huttel, Y. Thermal Diffusion at Nanoscale: From CoAu Alloy Nanoparticles to Co@Au Core/Shell Structures. *J. Phys. Chem. C* **2013**, *117*, 3101−3108.
(36) Laio, A.; Gervasio, F. L. Metadynamics: a method to simulate rare events and reconstruct the free energy in biophysics, chemistry and material science. *Rep. Prog. Phys.* **2008**, *71*, 126601.
(37) Barducci, A.; Bonomi, M.; Parrinello, M. Metadynamics. *Wiley Interdiscip. Rev. Comput. Mol. Sci.* **2011**, *1*, 826−843.
(38) Sutto, L.; Marsili, S.; Gervasio, F. L. New advances in metadynamics. *Wiley Interdiscip. Rev. Comput. Mol. Sci.* **2012**, *2*, 771−779.
(39) Mariscal, M. M.; Mayoral, A.; Olmos-Asar, J. A.; Magen, C.; Mejía-Rosales, S.; Pérez-Tijerina, E.; José-Yacamán, M. Nanoalloying in real time. A high resolution STEM and computer simulation study. *Nanoscale* **2011**, *3*, 5013.
(40) Paz, S. A.; Leiva, E. P. M.; Jellinek, J.; Mariscal, M. M. Properties of rotating nanoalloys formed by cluster collision: A computer simulation study. *J. Chem. Phys.* **2011**, *134*, 094701.
(41) Maragliano, L.; Vanden-Eijnden, E. A temperature accelerated method for sampling free energy and determining reaction pathways in rare events simulations. *Chem. Phys. Lett.* **2006**, *426*, 168−175.
(42) Abrams, C. F.; Vanden-Eijnden, E. Large-scale conformational sampling of proteins using temperature-accelerated molecular dynamics. *Proc. Natl. Acad. Sci. U. S. A.* **2010**, *107*, 4961−4966.
(43) Vashisth, H.; Storaska, A. J.; Neubig, R. R.; Brooks, C. L. Conformational Dynamics of a Regulator of G-Protein Signaling Protein Reveals a Mechanism of Allosteric Inhibition by a Small Molecule. *ACS Chem. Biol.* **2013**, *8*, 2778−2784.
(44) Lucid, J.; Meloni, S.; MacKernan, D.; Spohr, E.; Ciccotti, G. Probing the structures of hydrated nafion in different morphologies using temperature-accelerated molecular dynamics simulations. *J. Phys. Chem. C* **2013**, *117*, 774−782.
(45) Vashisth, H.; Abrams, C. F. All-atom structural models of insulin binding to the insulin receptor in the presence of a tandem hormone-binding element. *Proteins: Struct., Funct., Genet.* **2013**, *81*, 1017−1030.
(46) Zheng, L.; Chen, M.; Yang, W. Random walk in orthogonal space to achieve efficient free-energy simulation of complex systems. *Proc. Natl. Acad. Sci. U. S. A.* **2008**, *105*, 20227−20232.
(47) Zheng, L.; Chen, M.; Yang, W. Simultaneous escaping of explicit and hidden free energy barriers: Application of the orthogonal space random walk strategy in generalized ensemble based conformational sampling. *J. Chem. Phys.* **2009**, *130*, 234105.
(48) Comer, J.; Phillips, J. C.; Schulten, K.; Chipot, C. Multiple-Replica Strategies for Free-Energy Calculations in NAMD: Multiple-Walker Adaptive Biasing Force and Walker Selection Rules. *J. Chem. Theory Comput.* **2014**, *10*, 5276−5285.
(49) Zhu, H.; Averback, R. Sintering processes of two nanoparticles: A study by molecular-dynamics simulations. *Philos. Mag. Lett.* **1996**, *73*, 27−33.
(50) Kart, H. H.; Wang, G.; Karaman, I.; Çagin, T. Molecular dynamics study of the coalescence of equal and unequal sized Cu nanoparticles. *Int. J. Mod. Phys. C* **2009**, *20*, 179−196.
(51) Ding, F.; Rosén, A.; Bolton, K. Size dependence of the coalescence and melting of iron clusters: A molecular-dynamics study. *Phys. Rev. B: Condens. Matter Mater. Phys.* **2004**, *70*, 075416.
(52) Grammatikopoulos, P.; Cassidy, C.; Singh, V.; Sowwan, M. Coalescence-induced crystallisation wave in Pd nanoparticles. *Sci. Rep.* **2015**, *4*, 5779.
(53) Arcidiacono, S.; Bieri, N.; Poulikakos, D.; Grigoropoulos, C. On the coalescence of gold nanoparticles. *Int. J. Multiphase Flow* **2004**, *30*, 979−994.
(54) Mariscal, M. M.; Dassie, S. A.; Leiva, E. P. M. Collision as a way of forming bimetallic nanoclusters of various structures and chemical compositions. *J. Chem. Phys.* **2005**, *123*, 184505.
(55) Chandross, M. Energetics of the formation of Cu-Ag core-shell nanoparticles. *Modell. Simul. Mater. Sci. Eng.* **2014**, *22*, 075012.
(56) Grammatikopoulos, P.; Kioseoglou, J.; Galea, A.; Vernieres, J.; Benelmekki, M.; Diaz, R. E.; Sowwan, M. Kinetic trapping through coalescence and the formation of patterned Ag-Cu nanoparticles. *Nanoscale* **2016**, *8*, 9780−9790.

DOI: 10.1021/acs.jctc.7b00151
J. Chem. Theory Comput. XXXX, XXX, XXX−XXX